ORIGINAL ARTICLE

Journal
the American Ceramic Society

The ionic conductivity of Sm-doped ceria

Julius Koettgen[1,2,3,4] (iD) | **Manfred Martin**[1,2,5,6] (iD)

[1]Institute of Physical Chemistry, RWTH Aachen University, Aachen, Germany

[2]JARA-HPC, Forschungszentrum Jülich and RWTH Aachen University, Aachen, Germany

[3]Materials Sciences Division, Lawrence Berkeley National Laboratory, Berkeley, CA, USA

[4]Department of Materials Science and Engineering, University of California, Berkeley, CA, USA

[5]Helmholtz-Institut Münster (IEK-12), Forschungszentrum Jülich GmbH, Münster, Germany

[6]JARA-Energy, Forschungszentrum Jülich and RWTH Aachen University, Aachen, Germany

Correspondence

Julius Koettgen, Institute of Physical Chemistry, RWTH Aachen University, Landoltweg 2, 52056 Aachen, Germany.
Email: julius.koettgen@rwth-aachen.de

Funding information

Basic Energy Sciences, Grant/Award Number: DE-AC02-05-CH11231

Abstract

The oxygen ion conductivity of polycrystalline samples of Sm-doped ceria and of Gd-doped ceria is studied as a function of doping fraction and temperature using impedance spectroscopy allowing the separation of bulk and grain boundary conductivity. The introduction of a fine spacing for the Sm dopant fraction allows the clear identification of the dopant fraction leading to the largest bulk conductivity. At 267°C, the largest bulk conductivity is shown for $Ce_{0.93}Sm_{0.07}O_{1.965}$. With increasing temperature, indications of an increase in the dopant fraction, which leads to the maximum in conductivity, are found. For the grain boundary conductivity, the maximum appears at larger dopant fractions compared to the bulk conductivity. The largest total conductivity for both dopants is again found for Sm-doped ceria. In literature, different syntheses and sample preparation methods led to larger total conductivities for Gd-doped ceria. In this work, we demonstrate that the variation of sintering conditions leads to scattering in the conductivity over one order of magnitude. Finally, we demonstrate that, in nominally pure cerium oxide, impurities dominate the ionic conductivity.

KEYWORDS

ceria, doping, ionic conductivity, impedance spectroscopy, grain boundary, impurities

1 | INTRODUCTION

Materials with a high oxygen ion conductivity are important for energy conversion, energy storage, and catalysis.[1–3] Solid oxide fuel cells (SOFC) and high-temperature electrolysis cells (SOEC) convert energy for storage and mobile applications.[4] Oxygen ion-conducting membranes can be applied in carbon capture and storage, as well as in catalysis.[5] For good performance, all of these applications require materials with a sufficiently high ionic conductivity. Yttria-stabilized zirconia (YSZ) is a commonly used material with a sufficiently high ionic conductivity around 900°C.[6,7] However, high operation

temperatures lead to enhanced degradation and thus lower lifespan of the fuel cells. Alternatively, cerium oxide (CeO_2, ceria) doped with a rare earth oxide (RE_2O_3) exhibits sufficiently high ionic conductivities around 600°C and is extensively investigated in literature, as reviewed in our earlier publication.[8] The high ionic conductivity is caused by both the creation of oxygen vacancies $V_O^{\bullet\bullet}$ by doping, as shown in Eq.1 in Kröger-Vink notation,[4] and weak defect-defect interactions.[8,9]

$$RE_2O_3 \rightarrow 2RE'_{Ce} + 3O_O^\times + V_O^{\bullet\bullet} \tag{1}$$
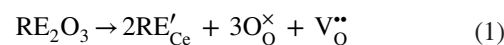
For a ternary cerium oxide, reports show that Sm-doped ceria ($Ce_{1-x}Sm_xO_{2-x/2}$) has one of the highest conductivities.

The total conductivity of polycrystalline Sm-doped ceria at 600°C according to several literature reports is shown in Figure 1 as a function of dopant fraction. The conductivity gains in value and subsequently decreases with increasing dopant fraction. The dopant fraction that can be associated with the maximum in conductivity is referred to as x_{max}. A summary of all x_{max} is shown in Table 1. Few reports do not show a monotonous decrease in conductivity with increasing dopant fraction x with $x > x_{max}$.[10,11] Grain size may affect this trend since grain sizes (100-500 nm) are comparably small in the work of Huang et al (Chem. Mater.).[12]

The total conductivity for polycrystalline samples is determined by the bulk and grain boundary contributions. Considering the bulk conductivity, oxygen ions jump within the regular oxygen sublattice of ceria. For grain boundary conduction, jumps take place in the grain boundary core and space charge zones as discussed in detail in literature.[13–18] The separation of both contributions is possible, for example, using impedance spectroscopy. Steele[19] showed the
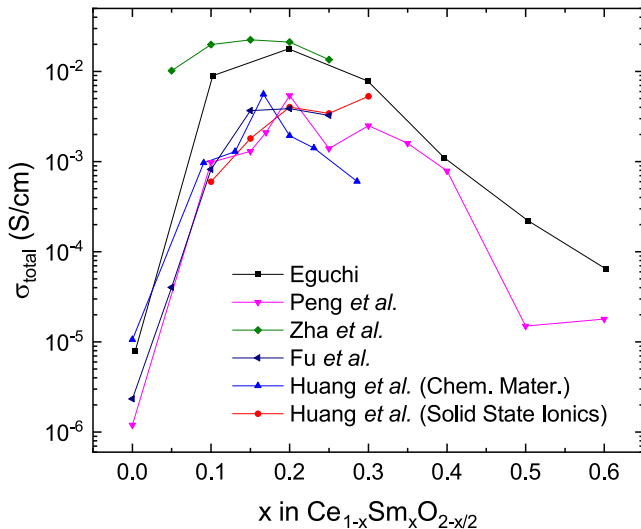

FIGURE 1 Total ionic conductivity of polycrystalline Sm-doped ceria at 600°C.[10,11,23,76,80] Lines are a guide to the eye only [Color figure can be viewed at wileyonlinelibrary.com]

TABLE 1 Dopant fractions leading to the highest total ionic conductivity for polycrystalline $Ce_{1-x_{max}}Sm_{x_{max}}O_{2-x_{max}/2}$ samples for given temperatures.[8]

Reference	x_{max}	Temperature [°C]
Yu et al[88]	0.12	230-900
Zha et al[23]	0.15	400-850
Huang et al (Chem. Mater.)[12]	0.17	200-600
Eguchi[80]	0.2	500-900
Huang et al (Solid state ionics)[10]	0.2-0.3	200-640
Peng et al[11]	0.2	600
Fu et al[76]	0.2	500-800

influences of bulk and grain boundary conductivity on the total conductivity of Gd-doped ceria at 500°C as a function of dopant fraction. The total conductivity is limited by the low grain boundary conductivity for small dopant fractions and by the low bulk conductivity for large dopant fractions. Compared to the total conductivity, x_{max} is small for the bulk conductivity. In the present work, the bulk conductivity is of particular interest as it represents the intrinsic property of the doped material largely without being influenced by the microstructure of the sample.

Bulk conductivities, however, were presented by only few groups for multiple Sm dopant fractions. Zhan et al[20] investigated polycrystalline ceria ($x = 0.1, 0.2, 0.3$) using impedance spectroscopy and found the largest conductivity for $x = 0.1$ for 250°C-550°C. Sanghavi et al[21] investigated single crystal thin films ($x = 0.074, 0.154, 0.27, 0.4$), which might share characteristics with the total conductivity due to its thin film properties, and found a maximum conductivity for $x = 0.154$ for 500°C-700°C. Both groups only chose very few dopant fractions with a coarse-grained spacing of $0.08 < \Delta x < 0.12$. At the same time, ionic conductivities can vary over one order of magnitude for $\Delta x = 0.1$. Therefore, in this work, we present bulk conductivities for a concentration series of Sm-doped ceria with a fine-grained spacing of the dopant fraction ($\Delta x \leq 0.025$). Beyond determining the optimal dopant fraction for applications, this work strives to enhance the understanding of the underlying mechanisms that define the influence of dopants on the ionic conductivity.

The structure of the paper is the following: The experimental setup and the impedance measurements are described in Section 2. In Section 3, the experimental results on the bulk and grain boundary conductivities of Sm-doped ceria as a function of temperature and doping with samarium are shown. We then compare our experimental results with our simulated ionic conductivities that were obtained by a combination of density functional theory calculations and Kinetic Monte Carlo (KMC) simulations. Finally, we compare the ionic conductivity in Sm- and Gd-doped ceria and give insight to the long-lasting discussion in literature, which dopant leads to the highest conductivity. A short summary is given in Section 4.

2 | EXPERIMENTAL DETAILS

Polycrystalline samples of the composition $Ce_{1-x}RE_xO_{2-x/2}$ were prepared according to the sol-gel method. The rare-earth (RE) cations Sm ($x = 0, 0.025, 0.05, 0.07, 0.075, 0.1, 0.125, 0.15, 0.2, 0.225,$ and 0.25) and Gd ($x = 0.07$ and 0.1) were used. Cerium (III) nitrate hexahydrate ($Ce(NO_3)_3 \cdot 6H_2O$, 99.9% Chempur), rare-earth (III) nitrate hydrate ($RE(NO_3)_3 \cdot 6H_2O$, 99.9%, Sm: Sigma-Aldrich, Gd: Strem Chemicals), and citric acid (VWR International, 2.5 equivalent) were dissolved in water. Minor errors in the stoichiometry are expected due

to the purity of the starting materials, though usage of the same batch for all samples only introduces a systematic error, which is similar for all samples. During mixing for several hours at 50°C, the sol-gel transformation occurred. The temperature was raised to 120°C-150°C leading to foaming. The foam was dried for 3 hours at 350°C and treated for 4 hours at 1000°C with a heating and cooling rate of 5°C/min. The powder was milled and uniaxially pressed to pellets with 10 mm diameter using a force of 25 kN for 25 minutes. The pellets were sintered in air at 1400°C for 24 hours with a heating and cooling rate of 200°C/hour.

Scanning electron microscope measurements (LEO 1450VP, Carl Zeiss) show that grain sizes are similar for the variously doped ceria (about 1 μm). The compositions of the pellets were successfully verified using energy dispersive X-ray spectroscopy measurements (Oxford INCA, Oxford Instruments). Using X-ray diffraction measurements (θ/θ-diffractometer, STOE & Cie GmbH with secondary monochromator or X'Pert Pro diffractometer, PANalytical, Almelo, Netherlands, with Ni-Filter),[22] the phase purity was investigated and the lattice parameters are in agreement to literature for Sm-[20,23] and Gd-doped ceria.[23,24] Especially, the long-lasting measurements with the X'Pert Pro diffractometer feature an outstanding resolution and signal-to-noise ratio ensuring the highly sensitive detection limit for impurities, which is required in this work.

Samples were covered and contacted with platinum paste and wire for impedance spectroscopy measurements. Samples were sintered at 1000°C for 3 hours (heating rate of 0.5°C/min and cooling rate of 0.9°C/min). Impedance spectroscopy measurements in air were performed using a Solatron 1260 (Schlumberger) and a 2-point geometry. The impedance was measured for frequencies between 10^7 and $7 \cdot 10^{-2}$ Hz. Between $7 \cdot 10^{-02}$ and 20 Hz, measurements were repeated five times and averaged. The impedance measurements were repeated for every composition with multiple samples and the excellent reproducibility for few temperatures was representatively verified.

Impedance measurements are often shown in the Nyquist plot (Figure 2), where the negative imaginary part as a function of the real part is given. The impedance of the solid electrolyte is compared to an electric circuit, which is then called equivalent circuit. JE Bauerle[25] proposed in the year 1969 an equivalent circuit for solid electrolytes consisting of a bulk, a grain boundary, and an electrode contribution. Although many other equivalent circuits have been proposed,[26] a modified variant of Bauerle's equivalent circuit model consisting of three serial resistor-capacitor circuits (RC circuit) is commonly used $(C_1/R_1 + C_2/R_2 + C_3/R_3)$ with resistances R_i and capacitances C_i. For pure and doped ceria, the bulk, grain boundary, and electrode contribution appear each as a semicircle in the Nyquist plot.[27–31] For the resulting equivalent circuit, the capacitance increases from bulk to electrode contribution.
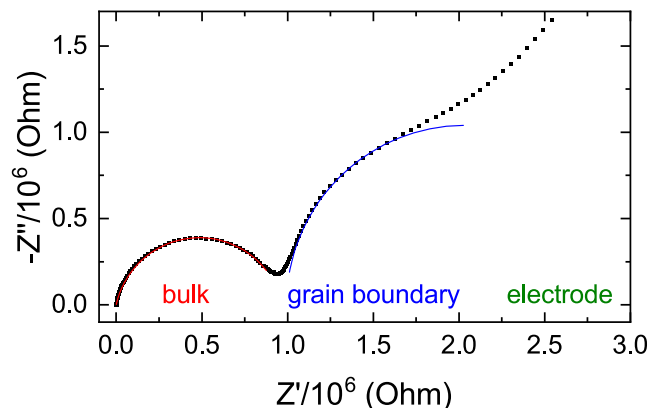

FIGURE 2 Nyquist plot with fitted equivalent circuit model for $Ce_{0.75}Sm_{0.25}O_{1.875}$ at 200°C [Color figure can be viewed at wileyonlinelibrary.com]

Rarely all contributions can be measured at the same time due to the limited frequency range in the experiment. Beyond that, interferences caused by other electric fields and overlapping semicircles appear. Therefore, in this work, every semicircle is fitted individually using the equivalent circuit model $R_1 + Q_2/R_2$. Fitting semicircles individually may lead to an overestimation of the resistance as compared for several measurements using one as well as two serial RC circuits: For the fit of individual semicircles, the resistance was overestimated up to 5% for the bulk conductivity and about 10% for the grain boundary conductivity. For dopant fractions above 10%, grain boundary and electrode semicircles significantly overlapped leading to an even larger error on the grain boundary conductivity. For most measurements, the centers of the semicircles were found to be below the x-axis, the semicircles appear flattened. The reason for this is the dispersion of physical properties in the sample. Therefore, instead of a capacitor, a constant phase element Q with the impedance $1/Z = (i\omega)^n Q$ was used for the equivalent circuit model.[27,32–35] For n = 1, the constant phase element is a capacitor. For smaller n, semicircles appear more flattened. Capacitance C and Q-value are connected using a pseudo-capacitance according to Hsu and Mansfeld.[36]

$$C = Q \cdot (\omega_{max})^{n-1} \qquad (2)$$

with the angular frequency ω_{max} at the vertex of the semicircle for which the imaginary part is a maximum. The semicircles are assigned according to their capacitance to the bulk and grain boundary contribution.[37] Few impedance spectra exhibit additional semicircles as discussed in literature.[20,38]

Impedance measurements were analyzed using EC-Lab (BioLogic) and a consecutive Randomize and Simplex-algorithm with similar results to a Marquardt-Levenberg algorithm. Ceria was investigated between 41°C and 750°C in steps of about 50°C. However, bulk conductivity could only be investigated up to 550°C (except for pure ceria up to 750°C)

and grain boundary conductivity only above 100°C due to the limited frequency range. In literature, bulk conductivities are often given for higher temperatures where the bulk resistance is calculated from the difference of the total resistance and the extrapolated grain boundary resistance. The contributions of the different contributions were assigned based on their pseudo-capacitance according to literature. The capacitance of the bulk contribution is in the range of tens of picofarads (10^{-11} F), which is consistent with the geometric capacitance of the samples according to literature. The capacitance of the grain boundary contribution is in the range of tens of nanofarads (10^{-8} F).[37,39,40]

The ionic conductivity is calculated according to

$$\sigma_i = \frac{l}{R_i \cdot A} \tag{3}$$

for the bulk and grain boundary conductivity, respectively, where R_i is the resistance according to the equivalent circuit, l the thickness of the sample, and A the electrode area. The same sample dimensions are used for bulk and grain boundary conductivity. In literature, also a specific grain boundary conductivity according to a brick layer model is calculated.[41] Errors arise due to the equivalent circuit fit, the thickness of the sample (±0.02 mm), and the diameter of the pellets. The resulting error in the conductivity (and stoichiometry) is mostly smaller than the symbol sizes used in this work. The prefactor of conductivity, A, and the activation enthalpy, ΔH_a, were determined according to the Arrhenius relation $\sigma_i = \frac{A}{T}e^{-\frac{\Delta H_a}{k_B T}}$. For selected samples, the conductivity behavior is divided into temperature regions according to literature.[20,42].

According to the serial brick layer model, the total resistivity is the sum of the macroscopic resistivities of bulk and grain boundary contribution, $R_{total} = R_{bulk} + R_{gb}$.[25,43–45] Therefore, the total conductivity

$$\sigma_{total} = \frac{l/A}{R_{bulk} + R_{gb}} \tag{4}$$

is always dominated by the higher resistivity or the lower conductivity according to

$$\sigma_{total} = \frac{\sigma_{bulk} \cdot \sigma_{gb}}{\sigma_{bulk} + \sigma_{gb}}. \tag{5}$$

The prefactor of conductivity, the attempt frequency, and the activation enthalpy are determined from an Arrhenius plot according to an earlier work.[8]

3 | RESULTS AND DISCUSSION

3.1 | Sm-doped ceria

Bulk and (macroscopic) grain boundary conductivities of Sm-doped ceria are shown in an Arrhenius plot in Figure 3. The conductivities follow the commonly assumed Arrhenius behavior. Especially for the bulk conductivity, the Arrhenius fit can be significantly improved by separating the conductivities in a low and high temperature range. The resulting ΔH_a is higher in the low temperature region compared to the high temperature region. As a result, in the Arrhenius plot, a kink can be found. The kink in the conductivity is often assumed to correlate with the association energy of a dopant-oxygen vacancy pair in literature.[20,28,33,46–50] However, in our earlier work, we demonstrated that the association is actually a two-step process (catch-and-hold) and that the observed

(A) bulk contribution
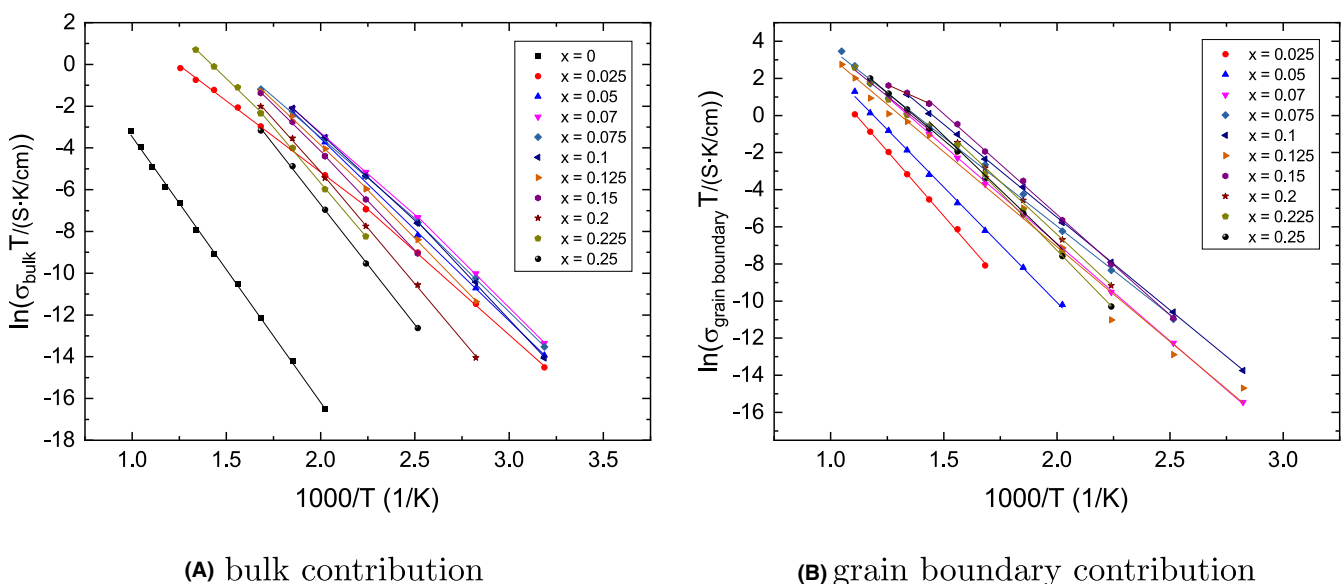
(B) grain boundary contribution

FIGURE 3 Arrhenius behavior of the ionic conductivity of the (a) bulk and (b) grain boundary contribution in $Ce_{1-x}Sm_xO_{2-x/2}$ according to impedance experiments [Color figure can be viewed at wileyonlinelibrary.com]

activation enthalpy difference is merely an effective association energy.[8]

The bulk conductivity shows the typical increase and subsequent decrease in conductivity with increasing dopant fraction (Figure 4). A maximum in the ionic conductivity can be found for $x = 0.07$. This is in agreement with the measurements of Zhan et al, who found a maximum for $x = 0.1$.[20] In literature, conductivities measured by different groups scatter for about one order of magnitude (see Figure 1). The main reason for the scattering is the strong influence of the synthesis and sample preparation on the conductivity though the underlying mechanism is still a topic of research.[51,52] We found that the bulk and grain boundary conductivities at 173°C of $Ce_{0.85}Sm_{0.15}O_{1.925}$ samples, which were sintered between 1111°C and 1514°C for between 4 and 55 hours, each scatter over one order of magnitude though no clear trend could be uncovered.

Figure 4 also shows that the bulk conductivities for the $x = 0.07$ and $x = 0.1$ compositions are similar above 200°C. The shift in the ratio between both conductivities indicates a shift of the dopant fraction of the maximum in conductivity x_{max} as found in experiments and simulations.[8] The higher thermal energy enhances the probability for oxygen vacancies to exit the association radius of the dopant ions (trapping). Furthermore, the probability of jumps around dopants that have a larger migration energy is enhanced (blocking).[8,53–55] Therefore, the maximum of the ionic conductivity is slightly shifted to larger dopant fractions. In conclusion, $Ce_{0.93}Sm_{0.07}O_{1.965}$ leads to the largest bulk conductivity for temperatures up to 267°C. Indications of an increase in the dopant fraction leading to the maximum in conductivity with increasing temperature can be found.

The separation of the grain boundary and electrode semicircle in the impedance spectrum of Sm-doped ceria with $x \geq 0.1$ is inaccurate due to the overlap of the semicircles, especially for $x = 0.125$. Therefore, all macroscopic grain boundary

conductivities with $x \geq 0.1$ may have a systematic error of one order of magnitude. Observed trends show a high degree of uncertainty. However, maxima at $x = 0.1$ and 0.15 and grain boundary conductivities $\sigma_{gb}(x)$ of $\sigma_{gb}(0.225) > \sigma_{gb}(0.25)$ for low temperatures and $\sigma_{gb}(0.225) < \sigma_{gb}(0.25)$ for high temperatures can be observed. The latter is even true for different fitting methods as described in the last section. The result is in agreement with literature, Zhan et al found a maximum in the grain boundary conductivity for $x = 0.1$ for low temperature.[20]

Additionally, ionic conductivities were simulated, as discussed in our earlier work,[8] using (KMC) simulations implemented in the software package iCon[56] based on migration energies from density functional theory calculations. While experiments and simulations are in general agreement for Sm-doped ceria, experimental conductivities for pure CeO_2 are significantly smaller than predicted by the KMC simulations. As our migration energy model in the KMC simulations should be best for pure ceria and small Sm dopant fractions, the discrepancy in conductivity may point out a fundamental difference between calculations and experiments. In fact, it is well known that in the experiments nominally pure ceria samples always contain small impurity amounts,[57–59] which lead to higher oxygen vacancy concentrations than intrinsic defects (anti-Frenkel) or defects caused by reduction at $p(O_2) = 0.2$bar for temperatures below 800°C.[60–63] Although often in literature no defect interactions for small dopant concentrations are expected,[8,57] experiments show a significant influence of the impurity level on the conductivity and activation enthalpy.[39] If these impurities are considered in the KMC simulations and are assumed to have a strong trapping effect,[64] for example, small amounts of Sc with a trapping energy of -0.65 eV as discussed in our earlier work,[8] the simulated ionic conductivity of nominally pure ceria decreases significantly. Figure 5 shows the conductivity for $Ce_{0.9999}Sc_{0.0001}O_{1.99995}$, which is in good agreement with the

(A) bulk contribution   **(B)** grain boundary contribution
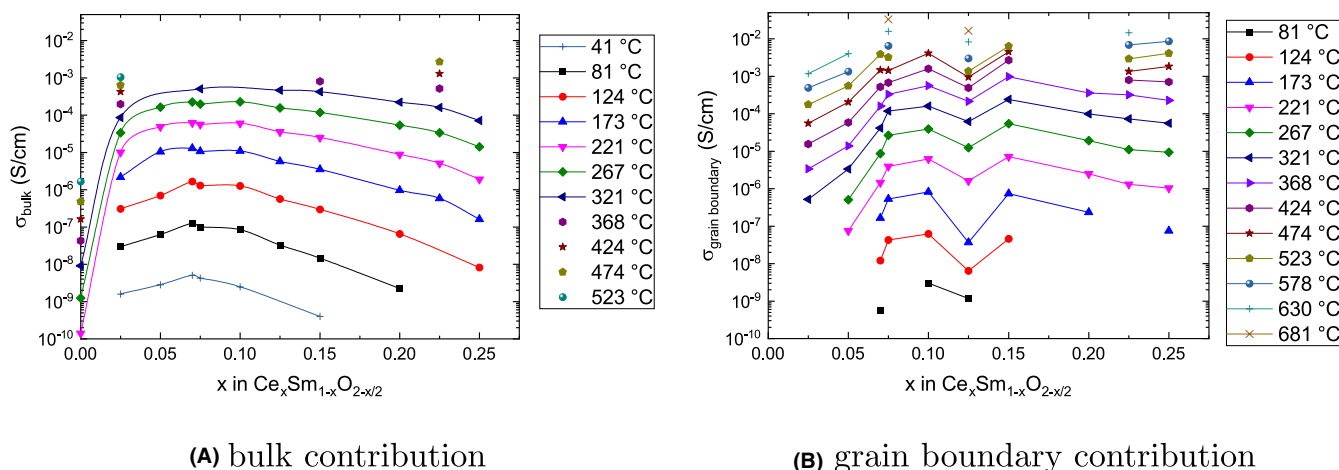
FIGURE 4 Ionic conductivity of the (a) bulk and (b) grain boundary contribution of Sm-doped ceria according to impedance experiments. Lines are a guide to the eye only [Color figure can be viewed at wileyonlinelibrary.com]

experiment. Therefore, we conclude that impurities dominate the ionic conductivities of nominally pure cerium oxides.

The experimental attempt frequency and activation enthalpy extracted from the Arrhenius behavior of the ionic conductivity according to an earlier work[8] is shown in Figure 6. Several trends similar to other experiments can be observed[8,57,65]: A decrease and subsequent increase of the activation enthalpy with increasing dopant fraction with a minimum at low dopant fractions can be found. However, the minimum in activation enthalpy of the bulk contribution

at $x = 0.025$ appears at significantly lower dopant fractions compared to the maximum in ionic conductivity. This is in disagreement with the common assumption in literature that the activation enthalpy mirrors the maximum in the conductivity.[33,39,66–68]

Activation enthalpies for the high temperature region are always smaller (about 0.1 eV) than for the low temperature region in agreement with literature.[20,28,33,46–50]

3.2 | The best dopant: Sm or Gd?

For a long time, it has been discussed in literature, which rare-earth (RE)-doped ceria, using only a single dopant, leads to the best ionic conductivity.[4] In fact, there is no plain answer to this question since the ionic conductivity not only depends on the kind of dopant but also on the dopant fraction, the measured temperature, and the choice between total and bulk conductivity. In literature, the conductivity of $Ce_{0.8}RE_{0.2}O_{1.9}$ at possible application temperatures is used as a first indication to choose the optimal dopant. Conductivities for the total[69–72] and bulk conductivity[24,33,35,46,49,73–75] suggest a high conductivity for Sm- and Gd-doped ceria.

The total conductivity for 600°C in polycrystalline Sm- and Gd-doped ceria is shown in Figure 7. Huang et al,[10,12] Peng et al,[11] and Fu et al[76] investigated Sm-doped ceria for several dopant fractions leading to the lowest total conductivity, here. Significantly higher total conductivities were found by Kudo and Obayashi,[77,78] Hohnke,[79] Tianshu et al,[24] and Zha et al[23] for several dopant fractions of Gd-doped ceria. However, for $Ce_{0.8}RE_{0.2}O_{1.9}$ and sample preparation by the same group, the results of Eguchi et al[71] and Balazs and Glass[72] suggest higher conductivities for Sm-doped ceria.
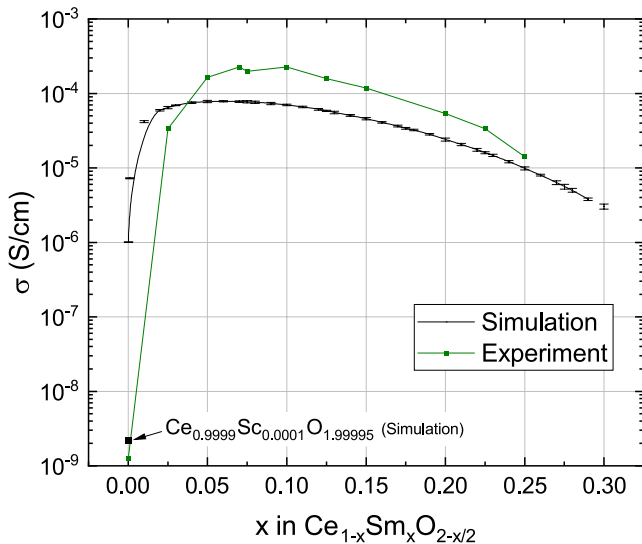

FIGURE 5 Simulated and experimental bulk ionic conductivities at 267°C of Sm-doped ceria as a function of doping fraction. In addition, the simulated ionic conductivity of $Ce_{0.9999}Sc_{0.0001}O_{1.99995}$ is shown. Lines are a guide to the eye only.[8] Reproduced by permission of the PCCP OWNER SOCIETIES [Color figure can be viewed at wileyonlinelibrary.com]
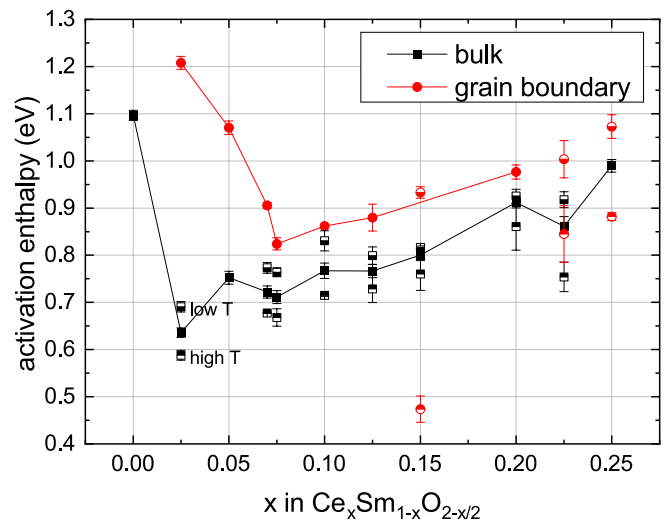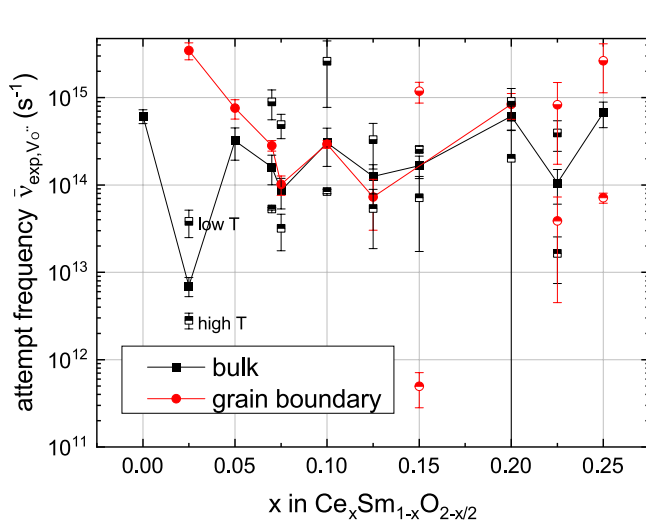

FIGURE 6 Experimental attempt frequency (left) and activation enthalpy (right) of Sm-doped ceria for all temperatures (solid symbols) or low and high temperatures according to impedance experiments. Lines are a guide to the eye only [Color figure can be viewed at wileyonlinelibrary.com]
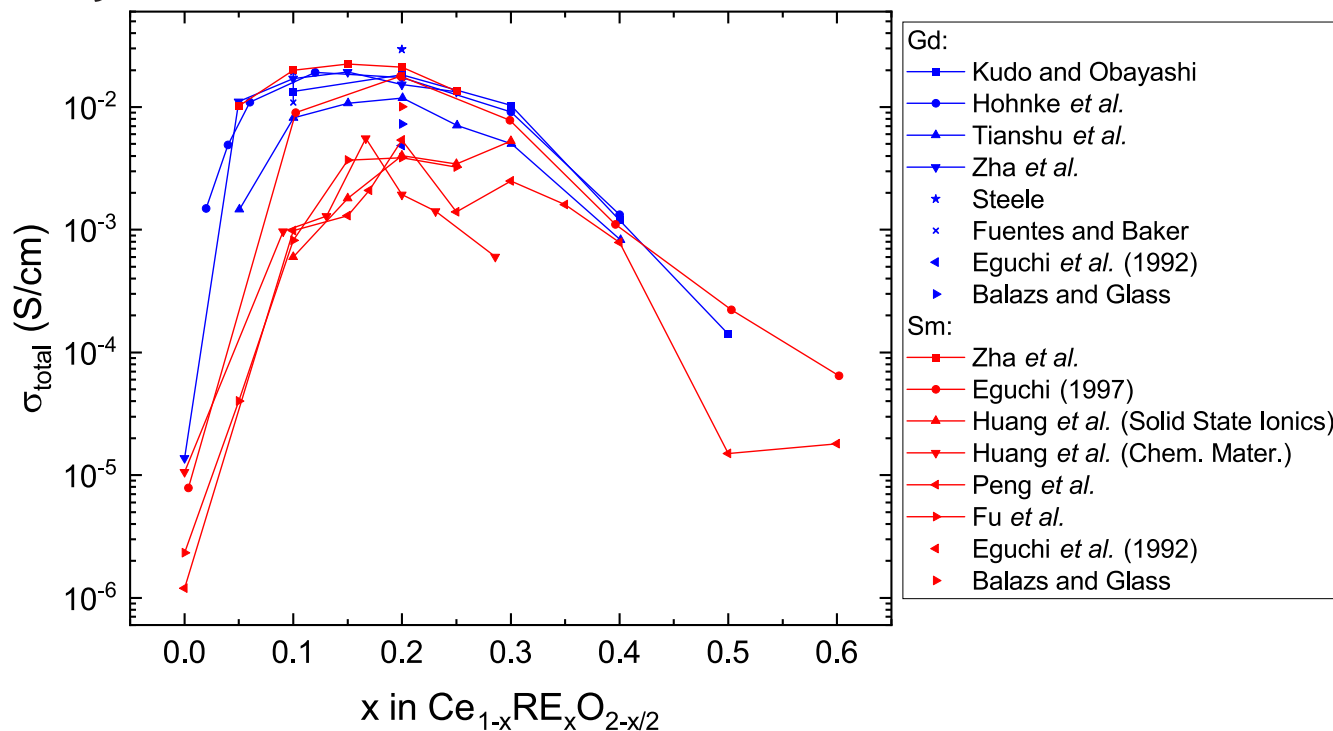
FIGURE 7 Total ionic conductivity of polycrystalline Sm- and Gd-doped ceria according to experiments at 600°C.[10–12,23,24,30,71,72,76,78–81] Lines are a guide to the eye only [Color figure can be viewed at wileyonlinelibrary.com]

Obviously, this discrepancy shows the strong influence of the sample synthesis and preparation. For instance, Fuentes and Baker[30] showed even higher total conductivities for $Ce_{0.9}Gd_{0.1}O_{1.95}$ between 0.011 and 0.019 S/cm. The results are again surpassed by the result of Zha et al[23] and especially Eguchi et al[80] for Sm-doped ceria. Still, the highest total conductivity is reported for $Ce_{0.9}Gd_{0.1}O_{1.95}$ by Steele.[81] This behavior may be related to the influence of the grain boundary contribution on the total conductivity as shown by Steele.[81] For a better understanding, bulk and grain boundary conductivity should be separated, for example, by using impedance spectroscopy.

The bulk conductivities for 500°C for Sm- and Gd-doped ceria are shown in Figure 8. Similar to the total conductivity, different research groups present different optimal dopants and dopant fractions. As discussed in the last section, these differences may be a result of different sample preparation techniques. Therefore, only similarly prepared Sm- and Gd-doped ceria should be compared. Similar compositions for both dopants were presented by several groups: Van Herle et al found similar conductivities for both dopants, Omar et al and Pérez-Coll et al found higher conductivities for Sm-doped ceria, Zajac and Molenda found higher conductivities for Gd-doped ceria.[26,33,40,47,82] However, Zajac and Molenda presented rather high conductivities compared to all other studies, which are therefore neglected in this study. As a result, the highest bulk conductivity in experiments at 500°C is

expected for Sm-doped ceria. This is in agreement with the simulations in our earlier publication.[8]

In this study, these results were analyzed in more detail. Therefore, dopant fractions at the maxima of the bulk conductivity (and grain boundary conductivity) for Sm-doped ceria were also investigated with Gd-doped ceria in impedance experiments. Of course, the maxima for Gd-doped ceria may be at different dopant fractions though Figures 7 and 8 suggest a similar curve progression. Therefore, the samples $Ce_{0.93}Sm_{0.07}O_{1.965}$ and $Ce_{0.9}Sm_{0.1}O_{1.95}$ (as discussed in the previous section) as well as $Ce_{0.93}Gd_{0.07}O_{1.965}$ and $Ce_{0.9}Gd_{0.1}O_{1.95}$ were investigated.

The bulk ionic conductivities of Sm- and Gd-doped ceria are shown in Figure 9. Conductivities from this work and literature are in agreement. Sm-doped ceria exhibits a larger bulk conductivity than Gd-doped ceria. The largest bulk conductivity is found for $Ce_{0.93}Sm_{0.07}O_{1.965}$. For Gd-doped ceria, doping with $x = 0.1$ leads to the higher bulk conductivity, which indicates a maximum at larger dopant fractions for Gd compared to Sm-doped ceria. This behavior was also predicted by our simulations and is due to the increased migration barriers for oxygen jumps around Gd dopants (blocking).[8] Above 200°C, the bulk conductivity of both investigated Sm-doped ceria compositions is similar. In summary, the largest bulk conductivity is found for $Ce_{0.93}Sm_{0.07}O_{1.965}$.

The macroscopic grain boundary conductivity, which is shown in Figure 10 (left), is generally several orders of magnitude smaller than the bulk conductivity. Only the bulk
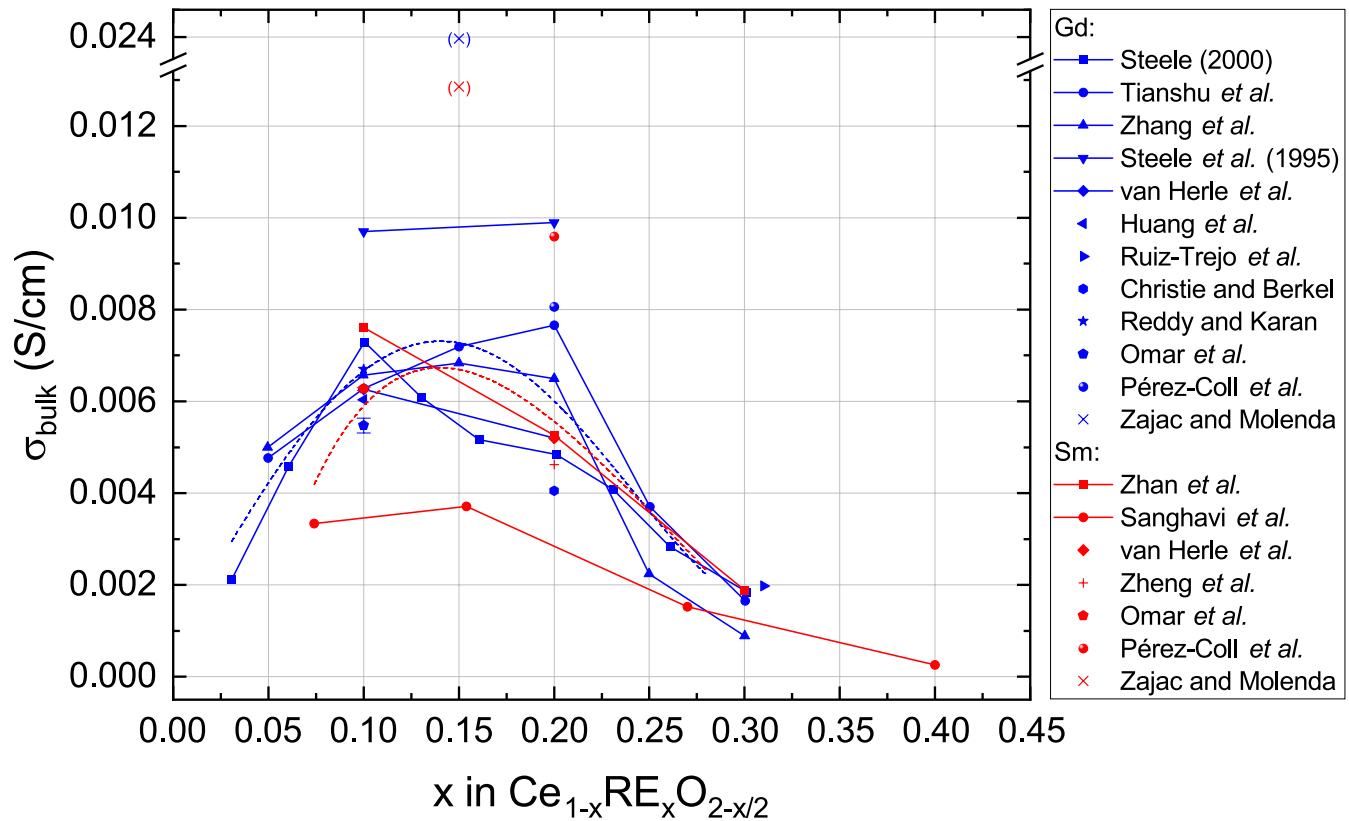
FIGURE 8 Bulk ionic conductivity of Sm-[20,21,26,33,40,47,50,82,85] and Gd-doped ceria[19,24,26–29,33,40,47,82,86,87] according to experiments at 500°C. Fourth-order polynomials were fitted to the data exempting the data of Zajac and Molenda to show the general trend of the data (dashed lines). Other lines are a guide to the eye only [Color figure can be viewed at wileyonlinelibrary.com]
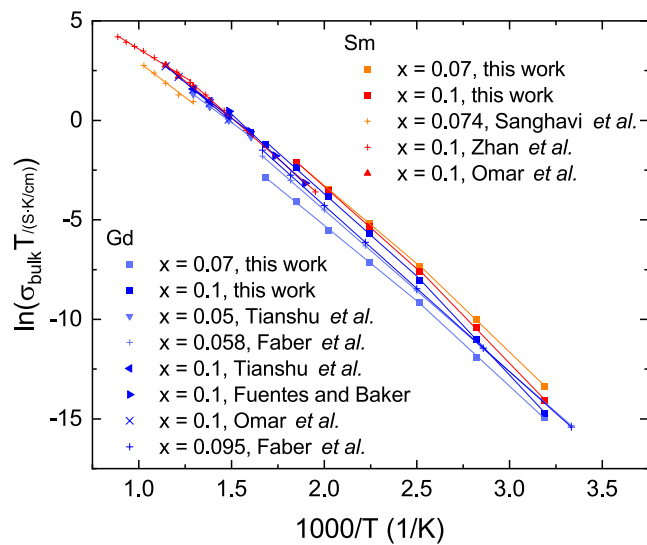

FIGURE 9 Bulk ionic conductivity of Sm- and Gd-doped ceria according to impedance experiments[20,21,24,30,47,67] [Color figure can be viewed at wileyonlinelibrary.com]

conductivity of $Ce_{0.93}Gd_{0.07}O_{1.965}$ above 250°C is similar to the grain boundary conductivity of 10% Sm- or Gd-doped ceria. As the activation energies for the grain boundary contribution are larger than for the bulk (see Figure 11), conductivities of both contributions may be similar around 800°C

and 1000°C. Especially for high dopant fractions, similar conductivities occur already at low temperature according to literature.[83] The ranking order for the grain boundary conductivity of both dopant fractions is different from the bulk conductivity. All 10% doped samples have larger grain boundary conductivities than the 7% doped ceria indicating a maximum at larger dopant fractions as seen in literature.[65] For both dopant fractions, Sm-doped ceria has the larger conductivity. In literature, the macroscopic grain boundary conductivity scatters even more than the bulk conductivity, though the measurements of Tianshu et al[24] are in good agreement with this work. The reasons for this scattering are the different syntheses and preparation methods as discussed before, which especially influence the grain boundary conductivity. As a result, the conductivities for $Ce_{0.9}Sm_{0.1}O_{1.95}$ according to Zhan et al[20] are significantly lower, thus $Ce_{0.9}Gd_{0.1}O_{1.95}$ according to Tianshu et al[24] and Fuentes et al[30] has larger conductivities.

The total conductivity (Figure 10 right) was calculated according to Equation 5. As the grain boundary conductivity is orders of magnitude smaller than the bulk conductivity in the investigated temperature range, the total conductivity is very similar to the grain boundary conductivity. Deviations between both increase with temperature are larger for Sm-doped ceria and are at least four times larger for the $x = 0.1$ dopant fractions. As a result, the activation enthalpy for the
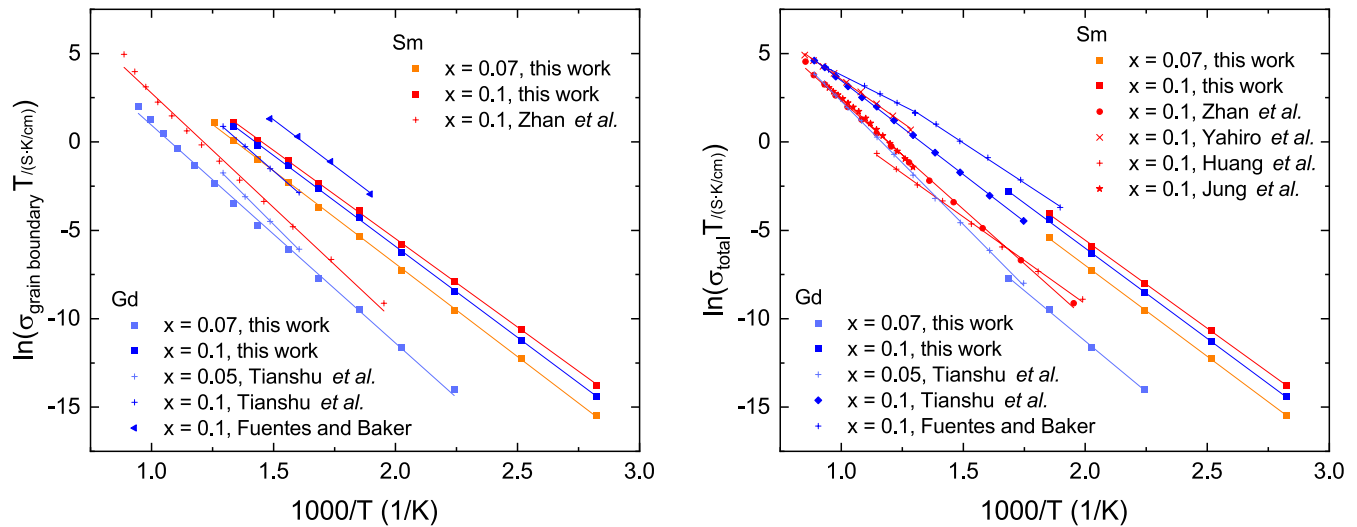
FIGURE 10 Grain boundary (left) and total ionic conductivity (right) of Sm- and Gd-doped ceria according to experiments[10,20,24,30,42,69] [Color figure can be viewed at wileyonlinelibrary.com]
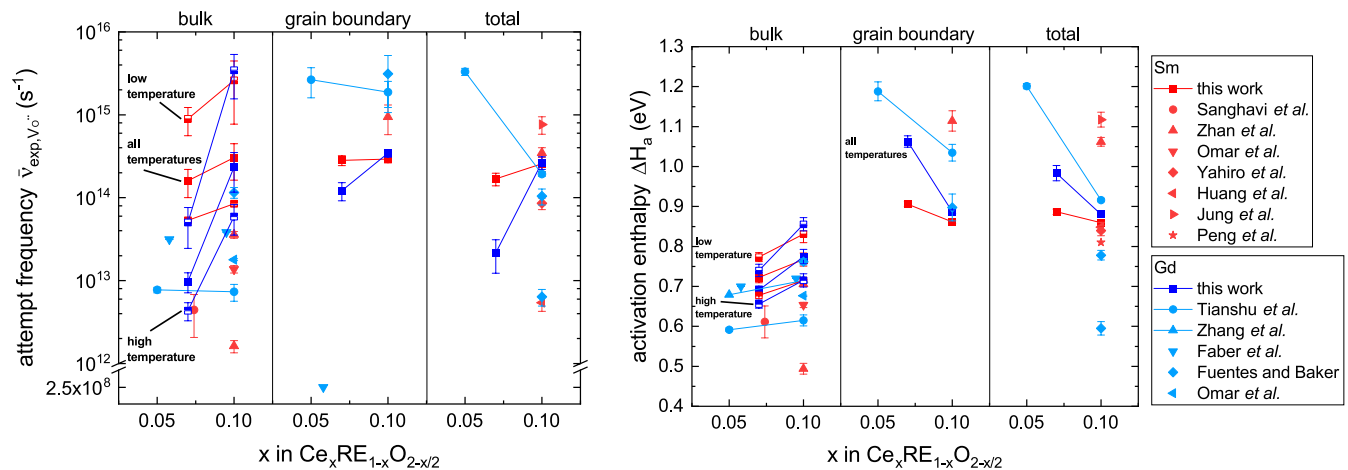

FIGURE 11 Experimental attempt frequency (left) and activation enthalpy (right) of Sm- and Gd-doped ceria according to experiments.[10,11,20,21,24,30,42,46,47,67,69] Lines are a guide to the eye only [Color figure can be viewed at wileyonlinelibrary.com]

total conductivity may change between the grain boundary-dominated low temperature region and the bulk-dominated high temperature region. Of course, a kink in the bulk conductivity due to association can also influence the total conductivity. In literature, Fuentes et al fit two activation enthalpies below and above 500°C.[30] Jung et al found significantly better regression coefficients using two straight lines for the Arrhenius plot though they do not use this result for their final evaluation.[42] Several other measurements could also be fitted with two temperature regions as shown in Figure 10. The strong scattering in the grain boundary conductivity propagates to the total conductivity. The total conductivities for the 10% dopant fraction scatters several orders of magnitude explaining the different results in literature for the best rare-earth dopant in ceria. In this work, $Ce_{0.9}Sm_{0.1}O_{1.95}$ shows the highest total conductivity, which

is in good agreement with Tianshu et al[24] and Yahiro et al[69] However, Fuentes and Baker[30] show higher conductivities for $Ce_{0.9}Gd_{0.1}O_{1.95}$. Figure 7 shows an increase in total conductivity for higher dopant fractions. In summary, the largest total conductivity is found for Sm-doped ceria. In literature, different syntheses and sample preparation methods lead to larger total conductivities for Gd-doped ceria.

The experimental attempt frequency and activation enthalpy of Sm- and Gd-doped ceria are summarized in Figure 11. Activation enthalpies in the grain boundary conductivity are significantly higher than in the bulk conductivity. While the activation enthalpy mostly increases for larger dopant fractions in the bulk conductivity, it mostly decreases in the grain boundary and total conductivity showing the high grain boundary activation enthalpy for $x < 0.075$. Activation enthalpies in Sm- and Gd-doped ceria are similar with the

exception of the grain boundary and total conductivity for $Ce_{0.93}Gd_{0.07}O_{1.965}$. Activation enthalpies in grain boundary and total conductivity are similar as the total conductivity is dominated by the grain boundary conductivity. Experimental attempt frequencies in the grain boundary conductivity are similar to the bulk conductivity except for $Ce_{0.93}Gd_{0.07}O_{1.965}$. In this work, the experimental attempt frequency increases for larger dopant fractions in the bulk, which propagates in the total conductivity, as the experimental attempt frequency is independent of dopant fraction in the grain boundary conductivity. According to Tianshu et al,[24] the experimental attempt frequency decreases for all contributions. Surprisingly, all experimental attempt frequencies for the grain boundary conductivity in this work are similar and low compared to literature. Experimental attempt frequencies in the total conductivity tend to be lower than in the grain boundary conductivity. This may be caused by an Arrhenius fit with a single activation enthalpy though one or more kinks in the conductivity are observed. Here, kinks result from a decrease in activation enthalpy for higher temperature due to either no longer existing association or change between grain boundary- and bulk-dominated total conductivity. Overall, both the experimental attempt frequency and activation enthalpy in this work are in agreement with literature. The best dopant, which leads to the highest conductivity, requires low activation enthalpies and high attempt frequencies. In this work, Sm-doped ceria fulfills both conditions though activation enthalpies and attempt frequencies are often very similar for Sm- and Gd-doped ceria.

4 | CONCLUSIONS

Impedance measurements were performed for Sm- and Gd-doped ceria to obtain the oxygen ion conductivities. Our experimental results agree well with literature, concerning both experimental results and theoretical results based on density functional theory calculations and (KMC) simulations. The introduction of a fine-grained spacing for the dopant fraction ($\Delta x \leq 0.025$) allows the identification of the optimal dopant fraction obtaining the maximum ionic conductivity. The largest bulk conductivity is found for $Ce_{0.93}Sm_{0.07}O_{1.965}$ between 41°C and 267°C.

Indications of an increase in the dopant fraction leading to the maximum in conductivity with increasing temperature are found. The maximum in ionic conductivity appears at larger dopant fractions in the grain boundary conductivity compared to the bulk conductivity. A strong influence of the sample preparation on the ionic conductivity was demonstrated: Bulk and grain boundary conductivities at 173°C of $Ce_{0.85}Sm_{0.15}O_{1.925}$ samples, which were sintered between 1111°C and 1514°C for between 4 and 55 hours, each scatter over one order of magnitude. Finally, impurities dominate the ionic conducthivity of nominally pure cerium oxides. Therefore, this work emphasizes the importance of controlled synthesis and sample preparation conditions.

In comparison with Gd-doped ceria, Sm-doped ceria leads to the largest bulk and total conductivity. While the largest bulk conductivity is found for $Ce_{0.93}Sm_{0.07}O_{1.965}$, the dopant fraction leading to the maximum in total conductivity is larger.

ORCID
Julius Koettgen https://orcid.org/0000-0002-8260-4793
Manfred Martin https://orcid.org/0000-0001-9046-050X

REFERENCES
1. Trovarelli A. Catalytic properties of ceria and CeO_2-containing materials. Catal Rev. 1996;38(4):439–520.
2. Hao Y, Yang CK, Haile SM. Ceria-zirconia solid solutions ($Ce_{1-x}Zr_xO_{2-\delta}$, $x \leq 0.2$) for solar thermochemical water splitting: a thermodynamic study. Chem Mater. 2014;26(20):6073–82.
3. Yang N, Shi Y, Schweiger S, Strelcov E, Belianinov A, Foglietti V, et al. Role of associated defects in oxygen ion conduction and surface exchange reaction for epitaxial samaria-doped ceria thin films as catalytic coatings. ACS Appl Mater Interfaces. 2016;8(23):14613–21.
4. Mogensen M. Physical, chemical and electrochemical properties of pure and doped ceria. Solid State Ion. 2000;129(1-4):63–94.
5. Gibbins J, Chalmers H. Carbon capture and storage. Energy Policy. 2008;36(12):4317–22.
6. Baumard JF, Abelard P. Defect structure and transport properties of ZrO2-based solid electrolytes. In: Rühle M, Claussen N, Heuer AH, editors. Science and technology of zirconia II. vol. v. 12 of advances in ceramics. Columbus, Ohio: American Ceramic Society; 1984. p. 555–71.
7. Arachi Y. Electrical conductivity of the ZrO_2–Ln_2O_3 (Ln = lanthanides) system. Solid State Ion. 1999;121(1–4):133–9.
8. Koettgen J, Grieshammer S, Hein P, Grope BOH, Nakayama M, Martin M. Understanding the ionic conductivity maximum in doped ceria: trapping and blocking. Phys Chem Chem Phys. 2018;20(21):14291–321.
9. Koettgen J, Martin M. Coordination numbers in Sm-doped ceria using x-ray absorption spectroscopy. J Phy Chem. 2019;123(11):6333–9.

10. Huang W. Properties of sol-gel prepared $Ce_{1-x}Sm_xO_{2-x/2}$ solid electrolytes. Solid State Ion. 1997;100(1–2):23–7.

11. Peng C, Zhang Y, Cheng ZW, Cheng X, Meng J. Nitrate–citrate combustion synthesis and properties of $Ce_{1-x}Sm_xO_{2-x/2}$ solid solutions. J Mater Sci-Mater El. 2002;13(12):757–62.

12. Huang W, Shuk P, Greenblatt M. Hydrothermal synthesis and properties of $Ce_{1-x}Sm_xO_{2-x/2}$ and $Ce_{1-x}Ca_xO_{2-x}$ solid solutions. Chem Mater. 1997;9(10):2240–5.

13. Kliewer KL, Koehler JS. Space charge in ionic crystals. I. general approach with application to NaCl. Phys Rev. 1965;140(4A):A1226–A1240.

14. Maier J, Reichert B. Ionic transport in heterogeneously and homogeneously doped thallium (I)-chloride. Berichte der Bunsengesellschaft für physikalische Chemie. 1986;90(8):666–70.

15. Bingham D, Tasker PW, Cormack AN. Simulated grain-boundary structures and ionic conductivity in tetragonal zirconia. Philos Mag. 1989;60(1):1–14.

16. Jamnik J, Maier J, Pejovnik S. Interfaces in solid ionic conductors: equilibrium and small signal picture. Solid State Ion. 1995;75:51–8.

17. Tschöpe A, Kilassonia S, Birringer R. The grain boundary effect in heavily doped cerium oxide. Solid State Ion. 2004;173(1–4):57–61.

18. De Souza RA. The formation of equilibrium space-charge zones at grain boundaries in the perovskite oxide SrTiO3. Phys Chem Chem Phys. 2009;11(43):9939–69.

19. Steele B. Appraisal of $Ce_{1-y}Gd_yO_{2-y/2}$ electrolytes for IT-SOFC operation at 500°C. Solid State Ion. 2000;129(1–4):95–110.

20. Zhan Z, Wen TL, Tu H, Lu ZY. AC Impedance investigation of samarium-doped ceria. J Electrochem Soc. 2001;148(5):A427.

21. Sanghavi R, Devanathan R, Nandasiri MI, Kuchibhatla S, Kovarik L, Thevuthasan S, et al. Integrated experimental and modeling study of the ionic conductivity of samaria-doped ceria thin films. Solid State Ion. 2011;205:13–9.

22. Leichtweiss T, Henning RA, Koettgen J, Schmidt RM, Holländer B, Martin M, et al. Amorphous and highly nonstoichiometric titania (TiO_x) thin films close to metal-like conductivity. J Mater Chem. 2014;2(18):6631.

23. Zha S, Xia C, Meng G. Effect of Gd (Sm) doping on properties of ceria electrolyte for solid oxide fuel cells. J Power Sources. 2003;115(1):44–8.

24. Tianshu Z, Hing P, Huang H, Kilner J. Ionic conductivity in the CeO_2–Gd_2O_3 system (0.05≤Gd/Ce≤0.4) prepared by oxalate co-precipitation. Solid State Ion. 2002;148(3–4):567–73.

25. Bauerle J. Study of solid electrolyte polarization by a complex admittance method. J Phys Chem Solids. 1969;30(12):2657–70.

26. van Herle J, Seneviratne D, McEvoy AJ. Lanthanide co-doping of solid electrolytes: AC conductivity behaviour. J Eur Ceram. 1999;19(6–7):837–41.

27. Christie G. Microstructure — ionic conductivity relationships in ceria-gadolinia electrolytes. Solid State Ion. 1996;83(1–2):17–27.

28. Huang K, Feng M, Goodenough JB. Synthesis and electrical properties of dense $Ce_{0.9}Gd_{0.1}O_{1.95}$ ceramics. J Am Cerami. 1998;81(2):357–62.

29. Reddy KR, Karan K. Sinterability, mechanical, microstructural, and electrical properties of gadolinium-doped ceria electrolyte for low-temperature solid oxide fuel cells. J Electroceram. 2005;15(1):45–56.

30. Fuentes RO, Baker RT. Structural, morphological and electrical properties of $Gd_{0.1}Ce_{0.9}O_{1.95}$ prepared by a citrate complexation method. J Power Sources. 2009;186(2):268–77.

31. Ding D, Liu B, Gong M, Liu X, Xia C. Electrical properties of samaria-doped ceria electrolytes from highly active powders. Electrochim Acta. 2010;55(15):4529–35.

32. Barsoukov E, Macdonald JR. Impedance spectroscopy: Theory, experiment, and applications, 2nd ed. Hoboken and N.J: Wiley-Interscience; 2005.

33. Pérez-Coll D, Marrero-López D, Núñez P, Piñol S, Frade JR. Grain boundary conductivity of $Ce_{0.8}Ln_{0.2}O_{2-\delta}$ ceramics (Ln=Y, La, Gd, Sm) with and without Co-doping. Electrochim Acta. 2006;51(28):6463–9.

34. Cioatera N, Pârvulescu V, Rolle A, Vannier RN. Effect of strontium addition on europium-doped ceria properties. Solid State Ion. 2009;180(9–10):681–7.

35. Sánchez-Bautista C, Dos santos-García AJ, Peña-Martínez J, Canales-Vázquez J. The grain boundary effect on dysprosium doped ceria. Solid State Ion. 2010;181(37–38):1665–73.

36. Hsu CH, Mansfeld F. Technical note: concerning the conversion of the constant phase element parameter Y_0 into a capacitance. Corrosion. 2001;57(9):747.

37. Wang DY, Nowick AS. The "grain-boundary effect" in doped ceria solid electrolytes. J Solid State Chem. 1980;35(3):325–33.

38. Eladham K, Hammou A. "Grain boundary effect" on ceria based solid solutions. Solid State Ion. 1983;10:905–12.

39. Wang D, Park D, Griffith J, Nowick A. Oxygen-ion conductivity and defect interactions in yttria-doped ceria. Solid State Ion. 1981;2(2):95–105.

40. Zajac W. Electrical conductivity of doubly doped ceria. Solid State Ion. 2008;179(1–6):154–8.

41. Haile SM, Staneff G, Ryu KH. Non-stoichiometry, grain boundary transport and chemical stability of proton conducting perovskites. Journal of Materials Science. 2001;36(5):1149–60.

42. Jung GB, Huang TJ, Chang CL. Effect of temperature and dopant concentration on the conductivity of samaria-doped ceria electrolyte. J Solid State Electrochem. 2002;6(4):225–30.

43. Beekmans NM, Heyne L. Correlation between impedance, microstructure and composition of calcia-stabilized zirconia. Electrochim Acta. 1976;21(4):303–10.

44. van Dijk T, Burggraaf AJ. Grain boundary effects on ionic conductivity in ceramic $Gd_xZr_{1-x}O_{2-(x/2)}$ solid solutions. Phys Status Solidi A. 1981;63(1):229–40.

45. Verkerk M, Middelhuis B, Burggraaf A. Effect of grain boundaries on the conductivity of high-purity ZrO_2-Y_2O_3 ceramics. Solid State Ion. 1982;6(2):159–70.

46. Zhang T, Ma J, Kong L, Chan S, Kilner J. Aging behavior and ionic conductivity of ceria-based ceramics: a comparative study. Solid State Ion. 2004;170(3–4):209–17.

47. Omar S, Wachsman ED, Jones JL, Nino JC. Crystal structure-ionic conductivity relationships in doped ceria systems. J Am Ceram Society. 2009;92(11):2674–81.

48. Pérez-Coll D, Núñez P, Frade JR. Improved conductivity of $Ce_{1-x}Sm_xO_{2-\delta}$ ceramics with submicrometer grain sizes. J Electrochem Society. 2006;153(3):A478.

49. Stephens I, Kilner J. Ionic conductivity of $Ce_{1-x}Nd_xO_{2-x/2}$. Solid State Ion. 2006;177(7–8):669–76.

50. Zheng Y, Zhou M, Ge L, Li S, Chen H, Guo L. Effect of Dy on the properties of Sm-doped ceria electrolyte for IT-SOFCs. J Alloys Compd. 2011;509(4):1244–8.

51. Bowman WJ, Zhu J, Sharma R, Crozier PA. Electrical conductivity and grain boundary composition of Gd-doped and Gd/Pr co-doped ceria. Solid State Ion. 2015;272:9–17.

52. Diercks DR, Tong J, Zhu H, Kee R, Baure G, Nino JC, et al. Three-dimensional quantification of composition and electrostatic potential at individual grain boundaries in doped ceria. J Mater Chem A. 2016;4:5167–75.

53. Grieshammer S, Grope BOH, Koettgen J, Martin M. A combined DFT + U and Monte Carlo study on rare earth doped ceria. Phys Chem Chem Phys. 2014;16(21):9974.

54. Lumeij M, Koettgen J, Gilleßen M, Itoh T, Dronskowski R. Detailed insights into the structural properties and oxygen-pathways in orthorhombic $Ba_{0.5}Sr_{0.5}Co_{0.8}Fe_{0.2}O_{3-\delta}$ by electronic-structure theory. Solid State Ion. 2012;223:53–8.

55. Koettgen J, Schmidt PC, Bučko T, Martin M. Ab initio calculation of the migration free energy of oxygen diffusion in pure and samarium-doped ceria. Phys Rev B. 2018;97(2):024305.

56. Hein P, Grope BOH, Koettgen J, Grieshammer S, Martin M. iCon: A general lattice Kinetic Monte Carlo program. submitted

57. Koettgen J, Zacherle T, Grieshammer S, Martin M. Ab initio calculation of the attempt frequency of oxygen diffusion in pure and samarium doped ceria. Phys Chem Chem Phys. 2017;19(15):9957–73.

58. Brugner FS, Blumenthal RN. Electrical conductivity of single-crystal CeO_2. J Am Ceram Society. 1971;54(1):57.

59. Blumenthal RN, Lee PW, Panlener RJ. Studies of the defect structure of nonstoichiometric cerium dioxide. J Electr Society. 1971;118(1):123.

60. Tuller HL. Defect structure and electrical properties of nonstoichiometric CeO_2 single crystals. J Electr Society. 1979;126(2):209.

61. Zacherle T, Schriever A, De Souza RA, Martin M. Ab initio analysis of the defect structure of ceria. Phys Rev B. 2013;87(13):134104.

62. Grieshammer S, Zacherle T, Martin M. Entropies of defect formation in ceria from first principles. Phys Chem Chem Phys. 2013;15(38):15935–42.

63. Martin M, Zacherle T, Schriever A, de Souza RA, Grieshammer S. Ab Initio calculation of the defect structure of ceria. ECS Transactions. 2013;57(1):2405–10.

64. Grieshammer S, Eisele S, Koettgen J. Modeling oxygen ion migration in the CeO_2–ZrO_2–Y_2O_3 solid solution. J Phys Chem C. 2018;122(33):18809–17.

65. Köttgen JR. The relation between defect interactions, local structure and oxygen ion conductivity in the bulk of doped ceria [PhD thesis]. Aachen: RWTH Aachen University; 2017.

66. Nowick AS, Wang DY, Park DS, Griffith J. Oxygen-ion conductivity and defect structure of CeO_2 doped with CaO and Y_2O_3. In: Fast ion transport in solids. Vashishta P, Mundy JN, Shenoy GK (eds). New York: North Holland; 1979: p. 673.

67. Faber J, Geoffroy C, Roux A, Sylvestre A, Abélard P. A Systematic investigation of the dc electrical conductivity of rare-earth doped ceria. Appl Phys A Solids and Surfaces. 1989;49(3):225–32.

68. Mori T, Buchanan R, Ou DR, Ye F, Kobayashi T, Kim J-D, et al. Design of nanostructured ceria-based solid electrolytes for development of IT-SOFC. J Solid State Electr. 2008;12(7–8):841–9.

69. Yahiro H, Eguchi Y, Eguchi K, Arai H. Oxygen ion conductivity of the ceria-samarium oxide system with fluorite structure. J Appl Electr. 1988;18(4):527–31.

70. Yahiro H. Electrical properties and reducibilities of ceria-rare earth oxide systems and their application to solid oxide fuel cell. Solid State Ion. 1989;36(1–2):71–5.

71. Eguchi K, Setoguchi T, Inoue T, Arai H. Electrical properties of ceria-based oxides and their application to solid oxide fuel cells. Solid State Ion. 1992;52(1–3):165–72.

72. Balazs G, Glass R. ac impedance studies of rare earth oxide doped ceria. Solid State Ion. 1995;76(1–2):155–62.

73. Li LP, Lin XM, Li GS, Inomata H. Solid solubility and transport properties of $Ce_{1-x}Nd_xO_{2-d}$ nanocrystalline solid solutions by a sol-gel route. J Mater Res. 2001;16(11):3207.

74. Aneflous L, Musso JA, Villain S, Gavarri JR, Benyaich H. Effects of temperature and Nd composition on non-linear transport properties in substituted $Ce_{1-x}Nd_xO_{2-\delta}$ cerium dioxides. J Solid State Chem. 2004;177(3):856–65.

75. Zhu JX, Zhou DF, Guo SR, Ye JF, Hao XF, Cao XQ, et al. Grain boundary conductivity of high purity neodymium-doped ceria nanosystem with and without the doping of molybdenum oxide. J Power Sources. 2007;174(1):114–23.

76. Fu YP, Wen SB, Lu CH. Preparation and characterization of samaria-doped ceria electrolyte materials for solid oxide fuel cells. J Am Ceram Society. 2008;91(1):127–31.

77. Kudo T, Obayashi H. Oxygen ion conduction of the fluorite-Type $Ce_{1-x}Ln_xO_{2-x/2}$ (Ln = Lanthanoid Element). J Electr Society. 1975;122(1):142.

78. Kudo T, Obayashi H. Mixed electrical conduction in the fluorite-type $Ce_{1-x}Gd_xO_{2-x/2}$. J Electr Society. 1976;123(3):415.

79. Hohnke DK. Ionic conduction in doped oxides with the fluorite structure. Solid State Ion. 1981;5:531–4.

80. Eguchi K. Ceramic materials containing rare earth oxides for solid oxide fuel cell. J Alloy Compd. 1997;250(1–2):486–91.

81. Steele BCH. Oxygen ion conductors. In: Takahashi T, editor. High conductivity solid ionic conductors. Singapore and Teaneck and N.J: World Scientific, 1989; p. 402–46.

82. Van herle J, Horita T, Kawada T, Sakai N, Yokokawa H, Dokiya M,.et al.Low temperature fabrication of (Y, Gd, Sm)-doped ceria electrolyte. Solid State Ion. 1996;88:1255–8.

83. Van herle J, Horita T, Kawada T, Sakai N, Yokokawa H, Dokiya M. Sintering behaviour and ionic conductivity of yttria-doped ceria. J Eur Ceram Society. 1996;16(9):961–73.

84. Jülich Supercomputing Centre. JURECA: general-purpose supercomputer at Jülich Supercomputing Centre. JLSRF. 2016;2:A62.

85. Bellino MG, Lamas DG, Walsöe de Reca NE. Enhanced ionic conductivity in nanostructured, heavily doped ceria ceramics. Adv Funct Mater. 2006;16(1):107–13.

86. Steele BCH, Zheng K, Rudkin RA, Kiratzis N, Cristie M. Properties and application of $Ce(Gd)O_{2-x}$ electrolytes in the temperature range 500°C-700°C. In: Dokiya M, editor. Proceedings of the fourth international symposium on solid oxide fuel cells (SOFC-IV). vol. 95–1 of proceedings of the electrochemical society. Pennington, NJ: Electrochemical Society; 1995. p. 1028–38.

87. Ruiz-Trejo E, Sirman JD, Baikov YM, Kilner JA. Oxygen ion diffusivity, surface exchange and ionic conductivity in single crystal Gadolinia doped Ceria. Solid State Ion. 1998;113–115(1–2):565–9.

88. Yu ZQ, Kuchibhatla SVNT, Saraf LV, Marina OA, Wang CM, Engelhard MH, et al. Conductivity of oriented samaria-doped ceria thin films grown by oxygen-plasma-assisted molecular beam epitaxy. Electr Solid St. 2008;11(5):B76.